Nanoscale

COMMUNICATION

View Article Online
View Journal | View Issue

Cite this: *Nanoscale*, 2018, **10**, 6806

Received 22nd December 2017,
Accepted 19th February 2018

DOI: 10.1039/c7nr09570h

rsc.li/nanoscale

Electrohydrodynamic printing of silver nanowires for flexible and stretchable electronics†

Zheng Cui,[a] Yiwei Han,[b] Qijin Huang,[a] Jingyan Dong*[b] and Yong Zhu *[a]

A silver nanowire (AgNW) based conductor is a promising component for flexible and stretchable electronics. A wide range of flexible/stretchable devices using AgNW conductors has been demonstrated recently. High-resolution, high-throughput printing of AgNWs remains a critical challenge. Electrohydrodynamic (EHD) printing has been developed as a promising technique to print different materials on a variety of substrates with high resolution. Here, AgNW ink was developed for EHD printing. The printed features can be controlled by several parameters including AgNW concentration, ink viscosity, printing speed, stand-off distance, *etc.* With this method, AgNW patterns can be printed on a range of substrates, *e.g.* paper, polyethylene terephthalate (PET), glass, polydimethylsiloxane (PDMS), *etc.* First, AgNW samples on PDMS were characterized under bending and stretching. Then AgNW heaters and electrocardiogram (ECG) electrodes were fabricated to demonstrate the potential of this printing technique for AgNW-based flexible and stretchable devices.

Flexible and stretchable conductors, a key component in flexible and stretchable electronics, have garnered significant attention from the scientific community and industry. Metal nanowires (NWs) in the form of random percolation network have shown excellent potential as flexible and stretchable conductors.[1–12] For a random network at a given material density, longer NWs can lead to higher electrical conductivity according to the percolation theory and larger stretchability, which are desirable for flexible and stretchable conductors. Longer NWs can also help in achieving a better balance between electrical conductivity and optical transmittance (*i.e.* increasing electrical conductivity without reducing optical transmittance), critical for transparent electrodes made of metal NWs.[5]

Printing is a powerful technique to enable the production of large-scale, low-cost electronic devices and systems. Most of the existing methods for fabricating metal NW conductors are based on solution coating and deposition, including drop casting, spin coating, spray coating, and Meyer rod coating.[1,13–15] Recently, contact printing methods such as gravure printing and screen printing have been reported for printing silver NWs (AgNWs).[16–18] While these methods can achieve high-speed and large-scale printing, the resolution and/or the electrical conductivity of the product is typically limited. Moreover, non-contact printing technologies that do not use a cliché have the advantage over contact printing of allowing on-demand patterning.

Inkjet printing, a representative form of non-contact printing, is widely used for printing electronic devices.[19–21] Ink-jet printing of long metal NWs (typically >10 μm), however, is challenging due to the risk of nozzle clogging and the difficulty in maintaining the structural integrity of the NWs through the printing process. The resolution of ink-jet printing technology is mainly limited by the size of the printer nozzle, with the printed droplets at the same scale of the nozzle size. For ink-jet printing as a general "rule of thumb", the size of the particles in the ink is suggested not to exceed 1/100 times the diameter of the printhead nozzle, so as to reduce the risk of nozzle clogging. Considering the length of typical AgNWs to be >10 μm, it is extremely difficult for inkjet printing to produce high-resolution features. Recently there have been a few studies of applying inkjet printing for metal NWs, however, the resolution in these studies is generally at a sub-mm scale, which is far from the requirement of advanced electronic devices. Electrohydro-dynamic (EHD) printing is an emerging technique that offers a high-resolution printing, which can produce jet or droplet that is much (up to a few orders of magnitude) smaller than the nozzle diameter. Due to this unique capability, large nozzle can be used in EHD printing to produce micro-scale features and also evade the dilemma of printing resolution and nozzle clogging.[22–25] Moreover, as a direct printing approach, EHD printing does not require a mask for device fabrication. EHD printing was recently used to print AgNWs. But that work focused on aligning AgNWs at very low NW density and the printed pattern was not conductive.[26]

[a]*Department of Mechanical and Aerospace Engineering, North Carolina State University, Raleigh, NC 27695, USA. E-mail: yong_zhu@ncsu.edu*
[b]*Department of Industrial and Systems Engineering, North Carolina State University, Raleigh, NC 27606, USA. E-mail: jdong@ncsu.edu*

†Electronic supplementary information (ESI) available. See DOI: 10.1039/c7nr09570h

Herein, we report high-resolution, large-scale printing of highly conductive AgNWs for flexible and stretchable electronics using EHD printing. AgNW ink was designed and synthesized for EHD printing. The smallest line width obtained in this work was ~45 μm. After post treatment, printed AgNWs showed an electrical conductivity as high as $\sim 5.6 \times 10^6$ S m^{-1}. Flexibility and stretchability of the printed patterns were characterized under cyclic bending and stretching tests. Devices based on the printed AgNWs were demonstrated including flexible heaters and stretchable dry electrodes for electrophysiology.

The EHD printing system included three sub-systems: a pneumatic dispensing system, a voltage supply system, and a precision three-axis translation stage. Fig. 1a shows the schematic of the printing system. The pneumatic system that includes an air pump, precision regulator was used to provide pressure to the AgNW solution to facilitate the ink flow from the printing nozzle. The voltage supply (Trek Model 610E, Trek, Inc.), providing a maximum voltage of 10 kV, was connected to the printing nozzle and the ground electrode on which the substrate sits. The precision three-axis stage was installed on an anti-vibration table to reduce vibrational noises. Three linear actuators were connected to the precision stage in XYZ directions, offering an accuracy of 100 nm in each direction. A side-view camera with a best resolution of 0.5 μm was used to monitor and record the printing process. Fig. 1c shows repeated patterns printed by EHD printing in a large scale, indicating the potential of this technique for large-scale, high-resolution printing of AgNW devices. Fig. 1D shows two examples of complicated patterns. More examples of patterns printed by EHD printing are shown in Fig. S2b, ESI.†

AgNW ink was synthesized and customized for EHD printing. Important ink parameters include viscosity and AgNW concentration. DI water was used as the major solvent. Poly (ethylene oxide) (PEO) was added to the ink to tune the viscosity. The rheological behavior of AgNW inks with different PEO concentrations (3%, 4%, and 5% weight ratio) was investigated. All three inks displayed a shear thinning thixotropic behavior. AgNW ink with a higher PEO concentration exhibited higher viscosity at the same shear rate. For instance, the viscosities at shear rate of 1 s^{-1} for the PEO concentration of 3%, 4% and 5% were 1.89, 4.28 and 8.61 Pa s, respectively (Fig. 2a). In this work, 4 wt% PEO was selected; the higher PEO concentration could cause nozzle clogging, while the lower concentration could reduce the printing resolution. The higher AgNW concentration can improve the conductivity of the printed pattern, but might cause AgNW clustering in the ink, increasing the possibility of nozzle clogging. On the other hand, the higher AgNW concentration might decrease the printing resolution as more NWs can be dragged out of the nozzle during printing (Fig. 2b). In this work, the AgNW concentration of 15 mg ml^{-1} was selected.

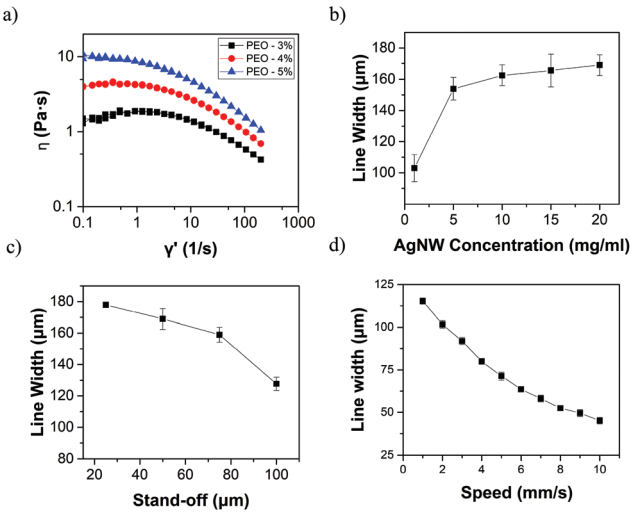

Fig. 2 (a) Shear viscosity for the three different AgNW ink formulations. Line width *vs.* (b) AgNW concentration in the inks, (c) stand-off distance and (d) printing speed.

The EHD printing process was affected by several parameters, including applied pressure, voltage, stand-off distance (distance between the printing head and the substrate), printing speed, and nozzle size. Due to the viscosity of the ink and relatively small nozzle used, a small air pressure of 0.4 psi was applied to the system to facilitate the ink flow to the nozzle tip. The applied voltage and the resulting electrostatic field played a crucial role in achieving the high printing resolution. Without the voltage, the ink just flowed out, and accumulated around the nozzle tip to form a ball shape, which produced large droplets leading to low-resolution printing. In this work, to initiate and maintain EHD printing, a voltage of 1500 V was applied between the nozzle and the ground electrode. The electrostatic force deformed the meniscus into a Taylor Cone, and ejected a fine jet from the Taylor Cone (Fig. 1b), leading to high-resolution printing. Dashed line indicates the external profile of the nozzle. Moreover, both the printing speed and the stand-off distance affected the printing resolution and the stability of the printing process. The higher printing speed and the larger stand-off distance provided better printing resolution. As shown in Fig. 2c, the line width decreased with the increasing stand-off distance, due to the reduced jet diameter from the Taylor Cone. In the rest of this work, a

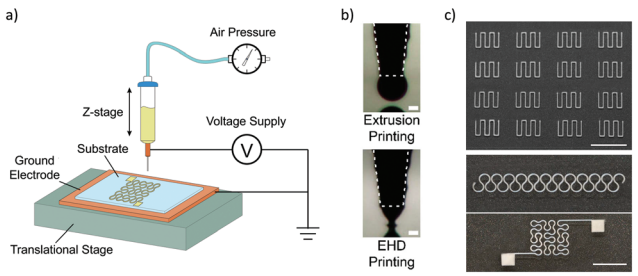

Fig. 1 (a) Schematic of the EHD printing setup. (b) Optical images of the EHD nozzle with voltage on and off, respectively. Scale bar, 100 μm. (c) Large-scale AgNW pattern printed by EHD printing. Scale bar, 1 cm. (d) Two complicated AgNW patterns with high resolution. Scale bar, 5 mm.

stand-off distance of 75 μm was selected. By increasing the printing speed, the line width decreased (Fig. 2d); at higher printing speed with the same ink flow rate, a smaller amount of ink per unit length leads to a smaller line width. Printed AgNW patterns had clean and smooth edges as shown in Fig. S2a, ESI,† which was essential for the circuit design, such as transistors and interdigitated sensors.

Next, we studied the morphology of the printed NW lines and the density of the NWs. The SEM images of the NWs at the center and the edge of the printed lines at two different printing speeds (high speed 10 mm s^{-1} and low speed 1 mm s^{-1}) are shown in Fig. 3. NW alignment and density can be evaluated from these images. In each case, the number of NWs under the same area was counted and the NW orientation was denoted from −90 to 90° with 0° pointing to the printing direction. It was observed that at the higher printing speed, most NWs (70%) are oriented from −10 to 10° with respect to the printing direction, slightly more aligned along the edges than at the center, due to the liquid drag force from high-speed printing. At the lower printing speed, NWs are distributed more randomly in the center, but more aligned in −10 to 10° along the edge. It is well known that the NWs are randomly oriented forming a percolation network when drop casted.[1,4] The alignment phenomenon observed above can be attributed to the shear flow. The shear flow along the liquid edge helps in achieving better NW alignment along the edge than at the center; the higher printing speed can result in better NW alignment due to higher shear flow rate. Table 1 shows the NW density at the center and along the edge. Here the NW density was calculated by counting the number of NWs in a fixed 50 × 50 μm square area.

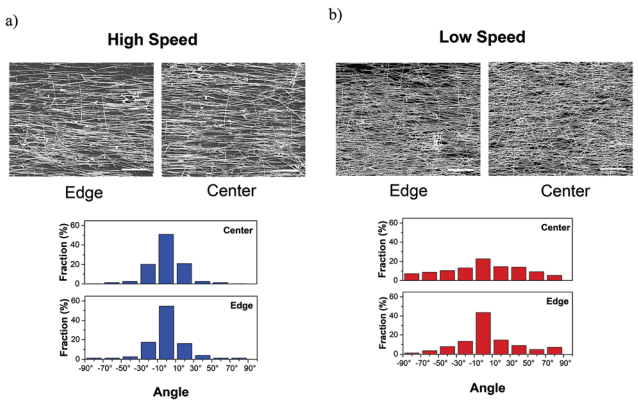

Fig. 3 AgNW alignment at the center and the edge of the printed line when printed at (a) high speed and (b) low speed. Scale bar is 10 μm.

Table 1 AgNW density at the center and along the edge at two different printing speeds

	Center [μm^2]	Edge [μm^2]
High-speed (10 mm s^{-1})	0.59	0.58
Low-speed (1 mm s^{-1})	1.86	1.30

Post treatment was performed to improve the conductivity of printed samples. Here, printed AgNW patterns were soaked in DI water for 5 min to remove PEO and then dried at 50 °C. This process may need to be repeated to remove PEO completely. After post treatment, the smallest line width achieved in this work was ~45 μm.

The electrical conductivity of the printed AgNW lines was characterized after the post treatment. The patterns used for the measurement had the same length of 10 mm but varying line width from 45 to 115 μm, controlled by the printing speed. Four-wire (4 W) measurement was used to measure the resistance of each sample accurately. AgNW lines with larger line widths possessed smaller resistances, as shown in Fig. 4a. Resistance, sheet resistance and conductivity of the samples were measured and calculated by the following method. Resistance was measured by the 4-wire measurement. Film thickness and the cross-sectional area were measured by using a Veeco Dektak 150 Profilometer (Fig. S5, ESI†). Sheet resistance R_s was calculated by $R_s = RW/L$ and electrical conductivity σ was calculated by $\sigma = L/(RA)$, where R, W, L and A are the measured resistance, the line width, the line length and the cross-sectional area, respectively. Fig. 4b and c show that as the line width increases, the pattern becomes more conductive. This is mainly because higher printing speed leads to lower density of NWs and hence lower electrical conductivity. NW alignment did not appear to play an important role in the electrical conductivity in this case. As mentioned earlier, when printing these lines, the only varying parameter was the printing speed, while all other parameters remained constant such as the AgNW concentration and the stand-off distance.

This EHD printing technique enables direct AgNW patterning on a variety of substrates with high resolution, as long as the substrate surfaces are hydrophilic for stable ink settlement. In this work, AgNW patterns were successfully printed on PDMS (dopamine treated), PET, glass, letter paper, nanofiber paper, polycarbonate filter (Whatman 111103) and nature rubber latex (lab use gloves).

Flexibility and stretchability of the printed AgNW conductors were evaluated, which are of importance relevance for their potential applications in wearable electronics. Bending and tensile tests of the printed AgNW conductors were carried out. AgNWs were printed on a flexible substrate, PET, for the bending tests. The bending angle started from 0° to 180° as shown in the inset of Fig. 5a. Given the thickness of the PET film of 0.12 mm, the maximum strain in the AgNWs at a bending angle of 180° was estimated to be 0.76% (smallest bending radius is ~2.7 mm). The sample showed a stable resistance reading with 200 cycles of repeated bending to the smallest bending radius of ~2.7 mm (Fig. 5b). Consecutive images showing the bending process can be found in Fig. S3.† For the tensile tests (Fig. 5c), AgNWs were printed on a PDMS substrate that was pre-strained at 50%, which was then released after the post treatment of the printed AgNWs. This pre-straining/releasing step was to generate a wavy AgNW/PDMS structure, which is a commonly used strategy to generate stretchable conductors with nearly constant resistance during sub-

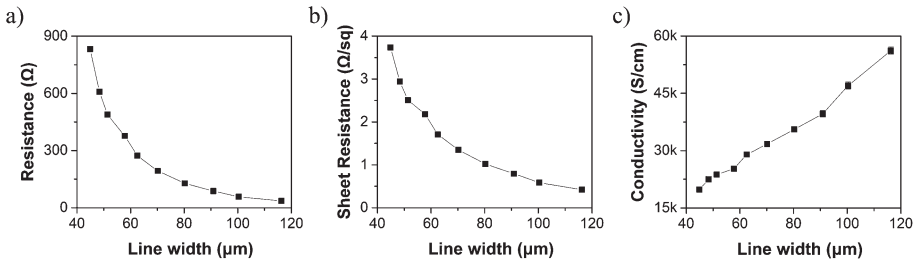

Fig. 4 Electrical properties of printed AgNW lines with different line widths including (a) resistance, (b) sheet resistance, and (c) conductivity.

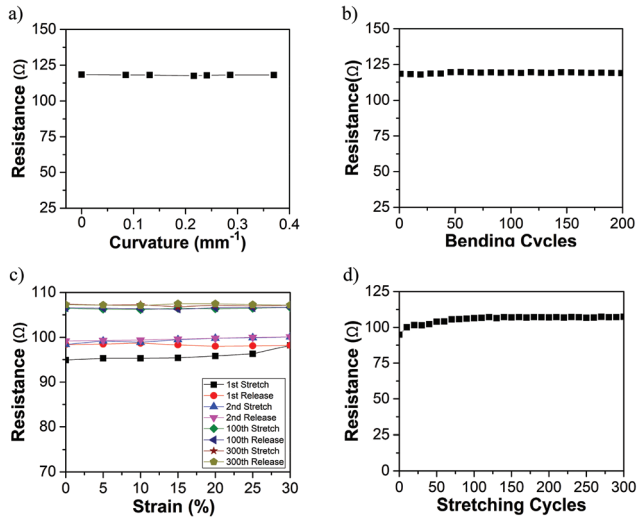

Fig. 5 Stable resistance of printed AgNW patterns under bending and stretching tests. (a) Resistance as a function of bending curvature. (b) Resistance under 200 bending cycles with a bending curvature of 0.37 mm^{-1} or a radius of 2.7 mm. (c) Resistance as a function of strain under selected stretching and releasing cycles. (d) Resistance under 300 stretching cycles with the maximum strain of 30%.

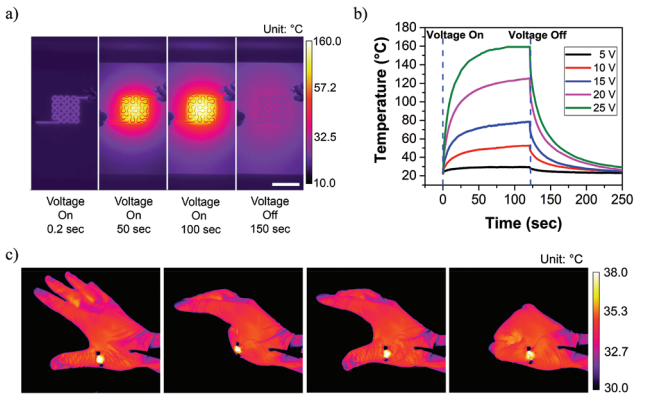

Fig. 6 Printed AgNW heaters. (a) IR images of a AgNW heater (scale bar, 5 mm). (b) Temperature *vs.* time for the AgNW heater in (a). (c) IR images of a AgNW heater directly printed on lab-use gloves.

sequent stretching. The as-prepared sample was then cyclic stretched to 30% strain and the resistance value was recorded simultaneously. At the beginning of the tests of the wavy AgNW conductor, the resistance increased a little with the increasing number of cycles (*i.e.* 10.6% increase in 50 cycles) (Fig. 5d). Afterwards, the resistance showed excellent stability. *In situ* SEM and optical images were taken during the tensile tests to capture the detailed AgNW/PDMS wavy structure and correlate with the resistance values (Fig. S4, ESI†). From the bending and tensile testing, the printed AgNW-based conductors exhibited excellent flexibility and stretchability, critical for many wearable device applications.[27–30]

The wearable heater is a promising candidate for thermal therapy.[31,32] In this work, the AgNW printed fractal pattern of Peano curves were demonstrated as a flexible heater. In the fractal pattern, arc sections replace the sharp corners from the mathematically defined fractal layout to improve the elastic mechanics (*e.g.* flexibility and stretchability). In addition, the fractal pattern of Peano curves can have large area coverage.[33] The footprint of the heater was 6 × 6 mm, as shown in Fig. 6a. Fig. 6a also shows several consecutively captured infrared (IR) images during an ON–OFF cycle. During the ON stage, a uniform temperature distribution was observed around the AgNW pattern. Fig. 6b shows the time-dependent temperature profile of the heater at different voltages. The maximum temperature obtained was ~160 °C at a voltage of 25 V, with the maximum heating rate and cooling rate of 21 and 29 °C S^{-1}, respectively. The same heater pattern was also directly printed on lab-use gloves to demonstrate the potential for wearable applications. The heaters exhibited stable heating performance when bent, stretched, and/or twisted. Fig. 6c shows the IR images of the heater under different deformation modes.

Dry ECG electrodes without the electrolytic gel layers as in the conventionally used wet electrodes have received significant interests for long-term health monitoring.[34,35] AgNW-based dry ECG electrodes have shown outstanding performances.[36] Here AgNWs were printed into a fractal pattern of Greek Cross, which also can effectively release the local strain under stretching, on PDMS substrates as the dry ECG electrodes (Fig. 7a).[33] The PDMS substrate has a thickness of 300 μm, enabling conformal contact between the skin and the conductive layer. As shown in Fig. 7b, the ECG signal captured from the printed AgNW dry electrode showed excellent performance compared to that obtained from the 3 M wet electrode. Since the printed AgNW electrodes are "dry" (*i.e.* without the electrolytic gel that can cause skin irritation under long-term wear), they are suitable for long-term ECG monitoring.

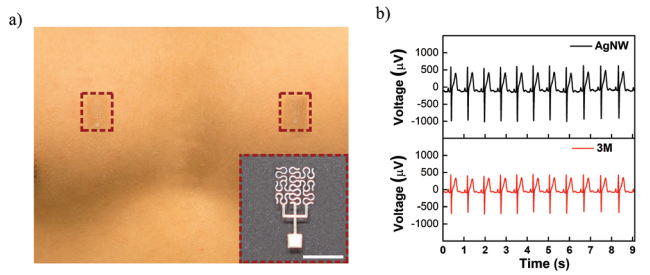

Fig. 7 Printed AgNW dry ECG electrodes. (a) Printed AgNW dry ECG electrodes mounted on chest. The inset shows a magnified image of an electrode. Scale bar, 5 mm. (b) ECG signals collected from the AgNW dry ECG electrode and a 3 M wet electrode for the purpose of comparison.

In summary, we report scalable, high-resolution and maskless printing of AgNWs using EHD printing. The EHD technique enables direct printing AgNWs on a diverse range of substrates, including PDMS, PET, glass, letter paper, nanofiber paper, and polycarbonate filter. The printed AgNW patterns were highly conductive (with conductivity as high as $\sim 5.6 \times 10^6$ S m^{-1}). The printed line width was found to depend on several ink and printing parameters, *e.g.*, ink viscosity, AgNW concentration, stand-off, printing speed, voltage, nozzle size, and pressure. The ink properties and printing conditions were characterized to achieve the optimal printing performance. Post treatment was developed to remove PEO residues and enhance the conductivity. A flexible heater was fabricated showing a uniform temperature distribution with a maximum heating rate of ~21 °C S^{-1} and a cooling rate of ~29 °C S^{-1}. The AgNW heater was also printed on lab-use gloves and showed stable heating performance under bending, stretching, and twisting. Printed AgNW dry ECG electrodes were able to collect accurate ECG signals, ideal for long-term wearable applications. Fractal-inspired patterns, such as Peano curve and Greek cross, were used to improve the elastic mechanics of the AgNW devices.

Experimental section

Ink preparation

The AgNW ink was obtained from mixing the AgNW solution (AgNW concentration is 150 mg ml^{-1} in DI water) and PEO solution. The AgNW used has an average diameter of ~120 nm and an average length of ~25 μm. The PEO powder (M_v: 1 000 000) was purchased from Sigma-Aldrich. The PEO powder was first diluted with DI water to form a PEO solution and then mixed it with AgNW solution and stirred for 10 min to achieve the AgNW inks with a AgNW concentration of 15 mg ml^{-1} and a PEO weight ratio of 4%.

AgNW pattern printing

Patterns were first created by using CAD software and then converted to the program code for printing. Printing parameters used for printing on glass slide substrate were as following: nozzle inner diameter of 150 μm (orifice of 150 μm), nozzle outer diameter of 250 μm, printing voltage of 1500 V, standoff distance of 75 μm, PEO concentration of 4%, AgNW concentration 15 mg ml^{-1}, and back pressure of 0.4 psi. Printing speed varies from 1–10 mm s^{-1} for various applications.

AgNW pattern post treatment and packaging

Printed AgNW patterns were first soaked in DI water for 5 minutes and then dried in an oven at 50 °C. This process needs to be repeated a few times to remove additives. Liquid metal (Gallium-Indium eutectic, Sigma Aldrich) and copper wires were used to form conformal electrodes, then covered with another layer of PDMS and cured.

Flexibility and stretchability characterization

AgNW patterns were printed on PET and PDMS for bending and stretching tests, respectively. The cyclic bending and stretching test was conducted on a custom-made testing stage. The four-wire measurement was used to measure the sample resistance under cyclic loading using a digital multimeter (34001A, Keysight Technologies).

Measurement of the heater and the test of the ECG

For the measurement of the heater, a DC power was applied to the heater at the two external pads. An IR thermometer (A655sc, FLIR) was used to measure the temperature distribution of the heater. For the ECG test, the as-fabricated electrodes were tested on a PowerLab 4/25 T (ADInstruments, Inc.) simultaneously with commercially available 3 M wet ECG electrodes for comparison. One 3 M electrode was the used ground/reference electrode; two pairs of the AgNW electrode and the 3 M electrode were attached to left and right chest, serving as positive and negative electrodes.

Author contributions

Z. C. and Y. H. performed and analyzed the experiments. Z. C. and Q. H. synthesized the silver nanowire used for printing. Y. Z. and J. D. conceived the research and provided guidance throughout the research. All authors discussed the results, co-wrote, and commented on the manuscript.

Conflicts of interest

There are no conflicts to declare.

Acknowledgements

The authors gratefully acknowledge financial support from the National Science Foundation (NSF) through Award No. CMMI-1728370 and CMMI-1333775. The authors would like to thank Dr G. Cheng for his help with the SEM imaging.

References

1 L. Hu, H. S. Kim, J.-Y. Lee, P. Peumans and Y. Cui, *ACS Nano*, 2010, **4**, 2955–2963.
2 S. De, T. M. Higgins, P. E. Lyons, E. M. Doherty, P. N. Nirmalraj, W. J. Blau, J. J. Boland and J. N. Coleman, *ACS Nano*, 2009, **3**, 1767–1774.
3 Z. Yu, Q. Zhang, L. Li, Q. Chen, X. Niu, J. Liu and Q. Pei, *Adv. Mater.*, 2011, **23**, 664–668.
4 F. Xu and Y. Zhu, *Adv. Mater.*, 2012, **24**, 5117–5122.
5 P. Lee, J. Lee, H. Lee, J. Yeo, S. Hong, K. H. Nam, D. Lee, S. S. Lee and S. H. Ko, *Adv. Mater.*, 2012, **24**, 3326–3332.
6 S. Gong, W. Schwalb, Y. Wang, Y. Chen, Y. Tang, J. Si, B. Shirinzadeh and W. Cheng, *Nat. Commun.*, 2014, **5**, 3132.
7 S. Yao and Y. Zhu, *Adv. Mater.*, 2015, **27**, 1480–1511.
8 I. Chang, T. Park, J. Lee, M. H. Lee, S. H. Ko and S. W. Cha, *J. Mater. Chem. A*, 2013, **1**, 8541–8546.
9 K. K. Kim, S. Hong, H. M. Cho, J. Lee, Y. D. Suh, J. Ham and S. H. Ko, *Nano Lett.*, 2015, **15**, 5240–5247.
10 Q. Zhang, Y. Di, C. M. Huard, L. J. Guo, J. Wei and J. Guo, *J. Mater. Chem. C*, 2015, **3**, 1528–1536.
11 J. Lee, K. An, P. Won, Y. Ka, H. Hwang, H. Moon, Y. Kwon, S. Hong, C. Kim, C. Lee and S. H. Ko, *Nanoscale*, 2017, **9**, 1978–1985.
12 Q. Zhang, W. Wei, J. Li, J. Wei and J. Guo, *Synth. Met.*, 2016, **221**, 192–200.
13 D. S. Leem, A. Edwards, M. Faist, J. Nelson, D. D. Bradley and J. C. de Mello, *Adv. Mater.*, 2011, **23**, 4371–4375.
14 M. Song, D. S. You, K. Lim, S. Park, S. Jung, C. S. Kim, D. H. Kim, D. G. Kim, J. K. Kim, J. Park, Y.-C. Kang, J. Heo, S.-H. Jin, J. H. Park and J.-W. Kang, *Adv. Funct. Mater.*, 2013, **23**, 4177–4184.
15 A. R. Madaria, A. Kumar and C. Zhou, *Nanotechnology*, 2011, **22**, 245201.
16 J. D. Park, S. Lim and H. Kim, *Thin Solid Films*, 2015, **586**, 70–75.
17 D. Angmo, T. R. Andersen, J. J. Bentzen, M. Helgesen, R. R. Søndergaard, M. Jørgensen, J. E. Carlé, E. Bundgaard and F. C. Krebs, *Adv. Funct. Mater.*, 2015, **25**, 4539–4547.
18 J. Liang, K. Tong and Q. Pei, *Adv. Mater.*, 2016, **28**, 5986–5996.
19 H. Lu, J. Lin, N. Wu, S. Nie, Q. Luo, C.-Q. Ma and Z. Cui, *Appl. Phys. Lett.*, 2015, **106**, 093302.
20 D. J. Finn, M. Lotya and J. N. Coleman, *ACS Appl. Mater. Interfaces*, 2015, **7**, 9254–9261.
21 R.-Z. Li, A. Hu, T. Zhang and K. D. Oakes, *ACS Appl. Mater. Interfaces*, 2014, **6**, 21721–21729.
22 S. Mishra, K. L. Barton, A. G. Alleyne, P. M. Ferreira and J. A. Rogers, *J. Micromech. Microeng.*, 2010, **20**, 095026.
23 C. Wei, H. Qin, N. A. Ramírez-Iglesias, C.-P. Chiu, Y.-s. Lee and J. Dong, *J. Micromech. Microeng.*, 2014, **24**, 045010.
24 Y. Han and J. Dong, *J. Micromech. Microeng.*, 2017, **27**, 035005.
25 J.-U. Park, M. Hardy, S. J. Kang, K. Barton, K. Adair, D. kishore Mukhopadhyay, C. Y. Lee, M. S. Strano, A. G. Alleyne, J. G. Georgiadis, P. M. Ferreira and J. A. Rogers, *Nat. Mater.*, 2007, **6**, 782.
26 H. Lee, B. Seong, J. Kim, Y. Jang and D. Byun, *Small*, 2014, **10**, 3918–3922.
27 W. Zeng, L. Shu, Q. Li, S. Chen, F. Wang and X. M. Tao, *Adv. Mater.*, 2014, **26**, 5310–5336.
28 J. A. Rogers, T. Someya and Y. Huang, *Science*, 2010, **327**, 1603–1607.
29 D. J. Lipomi, M. Vosgueritchian, B. C. Tee, S. L. Hellstrom, J. A. Lee, C. H. Fox and Z. Bao, *Nat. Nanotechnol.*, 2011, **6**, 788–792.
30 M. Park, J. Park and U. Jeong, *Nano Today*, 2014, **9**, 244–260.
31 S. Hong, H. Lee, J. Lee, J. Kwon, S. Han, Y. D. Suh, H. Cho, J. Shin, J. Yeo and S. H. Ko, *Adv. Mater.*, 2015, **27**, 4744–4751.
32 S. Choi, J. Park, W. Hyun, J. Kim, J. Kim, Y. B. Lee, C. Song, H. J. Hwang, J. H. Kim, T. Hyeon and D.-H. Kim, *ACS Nano*, 2015, **9**, 6626–6633.
33 J. A. Fan, W.-H. Yeo, Y. Su, Y. Hattori, W. Lee, S.-Y. Jung, Y. Zhang, Z. Liu, H. Cheng, L. Falgout, M. Bajema, T. Coleman, D. Gregoire, R. J. Larsen, Y. Huang and J. A. Rogers, *Nat. Commun.*, 2014, **5**, 3266.
34 S. Yao and Y. Zhu, *JOM*, 2016, **68**, 1145–1155.
35 K. I. Jang, H. N. Jung, J. W. Lee, S. Xu, Y. H. Liu, Y. Ma, J. W. Jeong, Y. M. Song, J. Kim, B. H. Kim, A. Banks, J. W. Kwak, Y. Yang, D. Shi, Z. Wei, X. Feng, U. Paik, Y. Huang, R. Ghaffari and J. A. Rogers, *Adv. Funct. Mater.*, 2016, **26**, 7281–7290.
36 A. C. Myers, H. Huang and Y. Zhu, *RSC Adv.*, 2015, **5**, 11627–11632.